Repeated Load Behavior of Continuously Reinforced Concrete Pavements

Erwin R. Kohler[1], Member ISCP and Jeffery R. Roesler[2], Member ISCP

Abstract

Full-scale test sections were constructed at the University of Illinois and subjected to accelerated pavement testing in order to evaluate IDOT's options on extended-life continuously reinforced concrete pavements (CRCP). The CRCP test sections included two concrete thicknesses, three steel contents, and the use of single versus double layer reinforcement. Response testing was first conducted on all the test sections in order to monitor the CRCP deformations under fixed loading and variable temperature conditions. Load levels were then applied at the edge of the pavement that would create a punchout failure on the test sections. The measured variables were the vertical and horizontal deformations at cracks and transverse strain near the surface of the slab, along with the temperature profile through slab thickness. The factors controlling the repeated load behavior of the CRC sections were the crack width, the permanent deformation of the support layers, and the steel content. The performance of the CRCP test sections exceeded existing design guide predictions. The main reason for the enhanced performance was the narrow crack width achieved on the test sections and resultant high shear capacity across the transverse cracks.

Introduction

Continuously Reinforced Concrete Pavements (CRCP) have shown to perform better than other types of concrete pavements (Gharaibeh et al. 1999, Smith et al. 1998) and are considered by some state agencies as the preferred option for extended life pavements for highways (Won 2005). The objective of the experiment described in this paper was to investigate the repeated load behavior of CRCP sections subjected to accelerated traffic loading in order to understand the mechanism of failure and to compare the performance of different design features.

Pavement sections for accelerated testing

Ten experimental sections were built at the Advanced Transportation Research and Engineering Laboratory (ATREL) in December 2001 with funding from the Illinois

---

[1] Postdoctoral Research Associate, Dept. of Civil and Environmental Eng., Univ. of Illinois, B233 NCEL, 205 N Mathews Ave., Urbana IL 61801 – ekohler@uiuc.edu

[2] Assistant Professor, Dept. of Civil and Environmental Eng., Univ. of Illinois, 1211 NCEL, 205 N Mathews Ave., Urbana IL 61801– jroesler@uiuc.edu

Department of Transportation. Sections 1 through 5 were loaded with accelerated traffic and the results are presented in this paper. Sections 6 to 10 were built to compare the effect of induced cracks on performance but have not yet been subjected to traffic. A summary of the benefits of active crack control for sections 6 to 10 versus the natural crack sections (1 through 5) can be obtained from Kohler and Roesler (2004a). All sections are approximately 26 m long with transition zones between sections designed to accommodate steel content changes, and restraints were constructed at the end of each lane to prevent excessive slab movement and to anchor the longitudinal steel. The end restraints consisted of a double lug system 3.66 m wide (same as the concrete pavement) and 1.22 m deep. The layout and main design characteristics of the sections are presented in Figure 1.

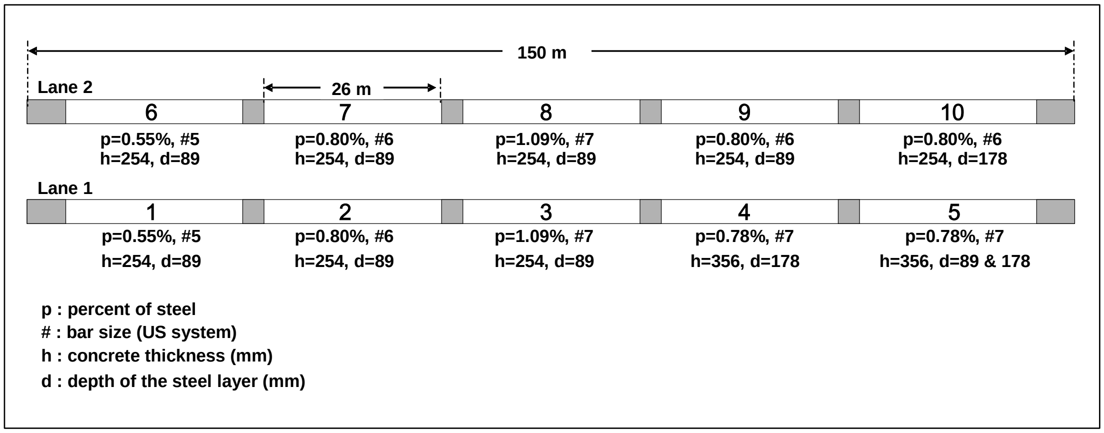

Figure 1. Layout and basic design parameters of test sections

All the transverse cracks in the pavement sections of this study developed naturally, i.e., there were no induced cracks in Lane 1 sections. The thickness of the concrete was 254 mm (10 inches) except in sections 4 and 5 where it was increased to 356 mm (14 inches). The slab reinforcement consisted of 26 longitudinal bars, spaced 140 mm apart. The bar diameter in sections 1 and 2 was 15.9 mm (#5) and 19.1 mm (#6), respectively. Sections 3 to 5 had 22.2mm bars (#7). The depth of the longitudinal reinforcement was 89 mm (3.5 inches) in sections 1 to 3, 114 mm in section 4, and the reinforcement was split in two layers in section 5, at 89 and 178 mm from the surface (3.5 and 7.0 inches). Transverse steel reinforcement (#4 bars) spaced every 1.2 m supported the longitudinal bars.

A variety of sensors were installed in the test sections in order to monitor the environmental and repeated load performance of the CRC pavement so that differences in pavement responses between test sections could be identified. The sensor arrangement used to capture the movements at the edge of the pavement is shown in Figure 2. Horizontal movements were measured, via LVDTs (linear variable displacement transducers), relative to each side of the crack, at different depths in the slab. Vertical movements were measured with two LVDTs suspended from a reference beam supported away from the loaded pavement edge. Vertical and horizontal sensors were placed concurrently at each monitored crack, as shown in Figure 3. During the CRC pavement construction, four strain gages were embedded in each section. The strain gages were placed 25 mm from the CRCP surface, oriented transversely, and at 1.3 m distance from the loaded edge, where the maximum stress was expected to occur under a rolling wheel. This distance was determined using the finite element analysis program, ILLISLAB. Thermocouples were placed at 25 mm from the top and bottom of the slab to determine the average pavement temperature and temperature differential. Additional thermocouples were monitored using the static data collection system which was independent of the dynamic loading system.

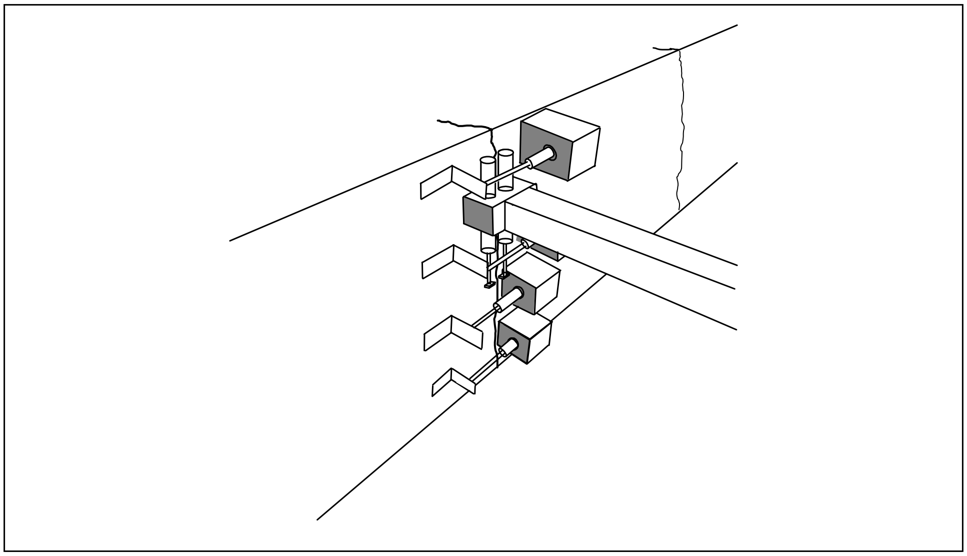

Figure 2. LVDT arrangement to measure crack movements at the edge

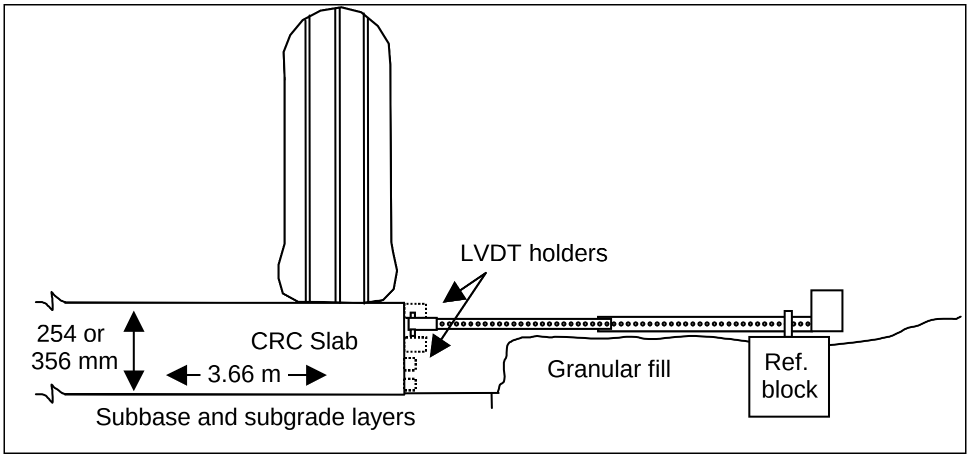

Figure 3. Cross-sectional view of loading and instrumentation at pavement edge

The full-scale pavement sections were loaded with the "Advanced Transportation Loading Assembly" (ATLAS). The ATLAS can apply vertical loads of up to 350 kN and can traverse the 26 m test section up to 16 km/h. A picture with a full view of the ATLAS device is shown in Figure 4.

Figure 4. ATLAS full view

The loading was primarily applied with a single aircraft tire with inflation pressure of 1.48 MPa. Most of the testing was done at a wheel speed between 9 and 13 km/h, under bi-directional trafficking mode, and at a fixed lateral position. To accelerate the pavement failure, the wheel load was applied along the edge of the pavement to produce the greatest deflection and stress. Pavement testing with the ATLAS started in August 2002 and lasted for two years. Section 1, 2, and 3 were tested to failure. Sections 4 and 5 were tested, though pavement failure was not achieved. The sections were tested in different seasons and consequently under different thermal conditions, as shown in Table 1.

Table 1. Dates of testing and pavement temperature range on experimental sections

Testing info	Section 1	Section 2	Section 4	Section 5	Section 3
Dates of testing(1)	6/16/02-6/23/03	6/30/03-9/13/03	1/3/04-3/6/04	4/6/04-4/15/04	5/26/04-8/4/04
Average pavement temperature	34-80 °F (2)	75-95°F	25-50°F	40-65°F	64-80°F

(1) It includes time when no load was being applied.

(2) Most of the testing was done during June 2003, when temperature was 60-80 °F

Response measurement and effect of temperature

Pavement responses under the action of the ATLAS wheel load were recorded continuously at each sensor along every section (one data point collected every 25 mm of wheel movement). Figure 5 shows an example of measured vertical deformations during a single wheel pass.

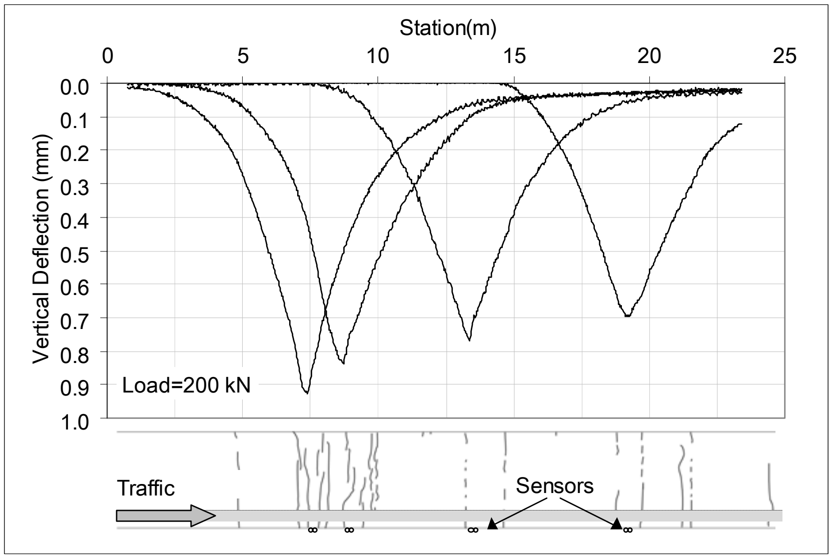

Figure 5. Vertical deflection measured during a single wheel pass

Similar influence lines were collected for transverse strains and for horizontal movements at the instrumented cracks. The effect of the moving wheel load is represented by the rebound responses, defined as the peak value measured as the wheel passes over the sensor compared to the reading after the wheel has moved away from the sensor. These responses depend on the load level being applied and are also function of the thermal state of the pavement, and they may vary along a section due to variability in the concrete material, local crack characteristics, and support conditions, as seen in Figure 5.

Figure 6 shows rebound vertical deflections measured continuously over a two-week period for a fixed load level of 133 kN. These measurements were obtained from section 3 during the summertime when the daily thermal cycles were more pronounced. Figure 6 also shows the temperature difference through the thickness of the slab, which fluctuated each day during this time of the year between -2 and 4°C approximately (note the temperature scale is inverted in the chart). The slab's temperature differentials were not as large as expected due to the sheltering effect of the ATLAS and the encapsulating tent structure. Despite the fixed load level, the rebound deflections were not constant but varied with thermal conditions in the slab. Deflections in the morning could be 20 percent higher than in the late afternoon.

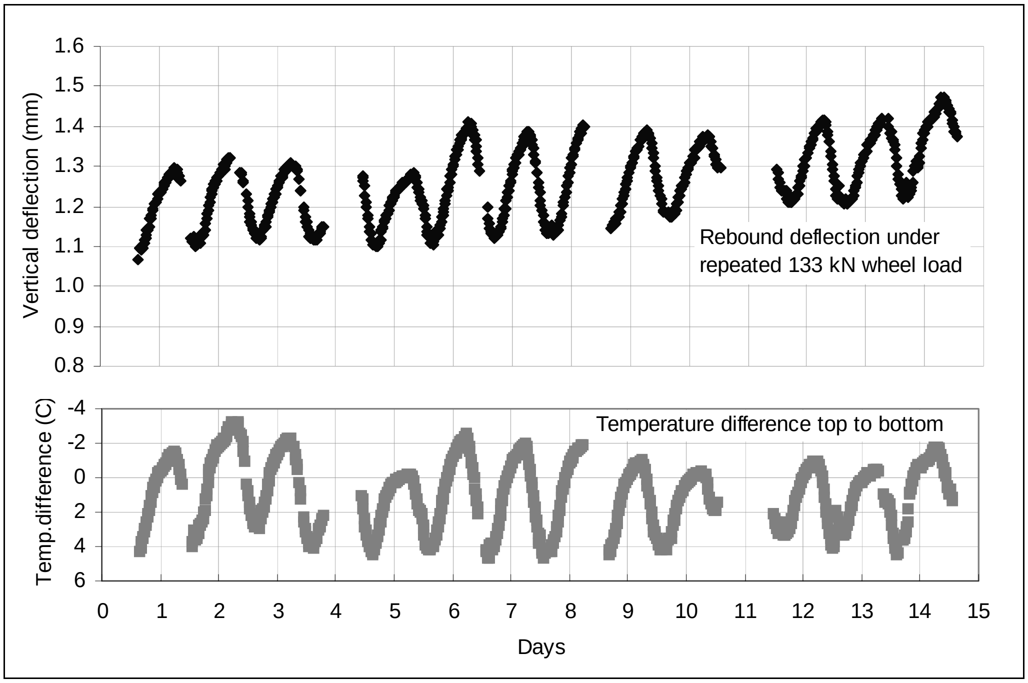

Figure 6. Variation in slab vertical deflection at a fixed load level due to changes in the slab's temperature differential

Transverse strain measurements for the same section and load level (133kN) are presented in Figure 7. The plot shows more scatter as the strain gage signals were not as clean as the LVDT's. Similar to the deflection measurements, the transverse bending strain, measured with embedded sensors at 1.3 m from the edge, increased with decreasing temperature differential. For instance, a variation of 40 microstrains measured 25mm below the slab surface can be observed within a few hours and is equivalent to approximately 2.4 MPa of additional tensile stress in the early morning with respect to the values during the afternoon.

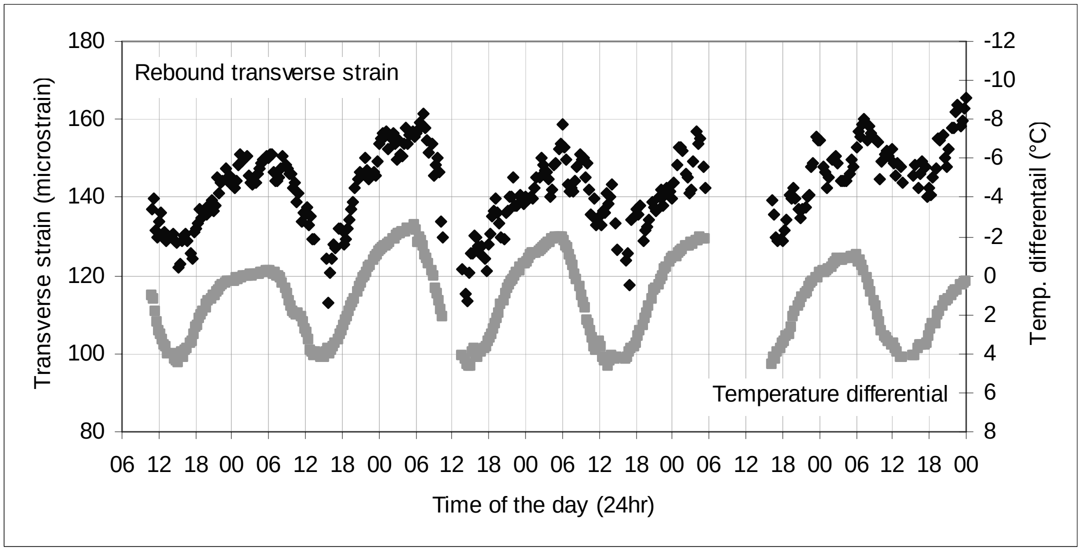

Figure 7. Hourly rebound transverse strain and slab temperature differential

Similar behavior was observed on all pavement sections where the transverse curling at the edge increased the rebound deflection and the transverse strain near the top of the slab. An example of the vertical displacement measured at the edge of the slab due to daily temperature cycles, with no applied wheel load, is shown in Figure 8. The data was gathered from section 1 during the month of September. In the early morning, when the temperature differential T_{diff} is about –4°C, the edge is lifted more than 0.20 mm. By 3 p.m. the edge has moved downward and remains down (possibly in full support) until T_{diff} become lower than about –1°C. The edge is then lifted up again during the night hours. The movement follows different paths during the periods of heating and cooling of the pavement, in a hysteretic behavior caused by the non-linearity of the thermal profile. Comparable results have been reported for in-service undoweled concrete pavements (Poblete et al. 1988).

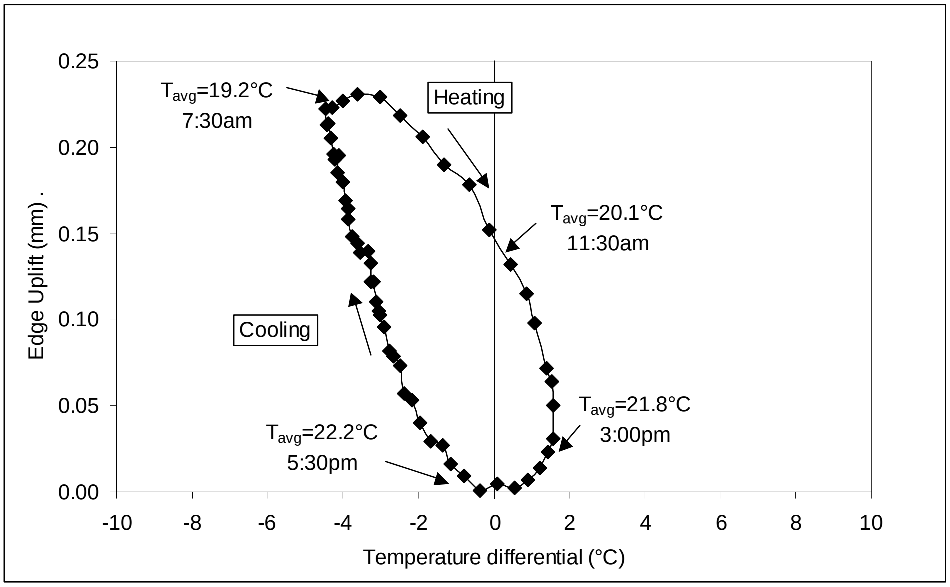

Figure 8. Edge uplift due to daily changes in temperature differential

The effect that the slab curling has on the pavement responses makes it difficult to compare strain and deflection measurements between sections that have been tested in different seasons. As a reference, Figure 9 shows typical temperature profiles measured in the pavement slab during winter and summer seasons and in the morning and in the afternoon hours.

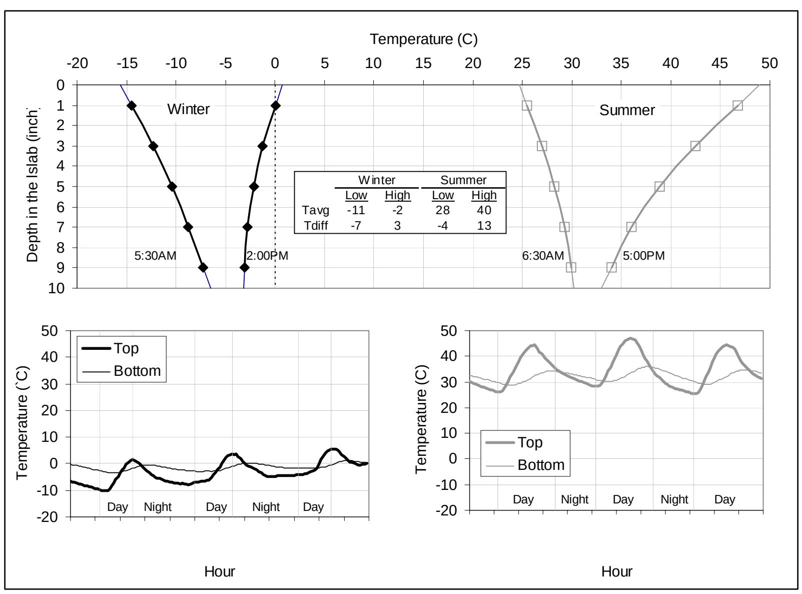

Figure 9. Pavement temperature profiles and daily temperature trends over three-day periods in winter and summer

Test section comparison based on elastic responses

The testing procedure followed in each section consisted of an initial loading at 45 kN to obtain elastic responses over a period of 24 hours, followed by heavy loading to accelerate pavement damage. The average vertical deflection under a 45 kN load for sections 1 through 5 are presented in Figure 10. Dispersion bars are included in the plot to account for the variability within the section, i.e., measurements at four different locations, and the aforementioned temperature effect. Typical temperatures ranges for Tavg and Tdiff are also presented in the chart in the form of representative ranges during the hours of testing in each section.

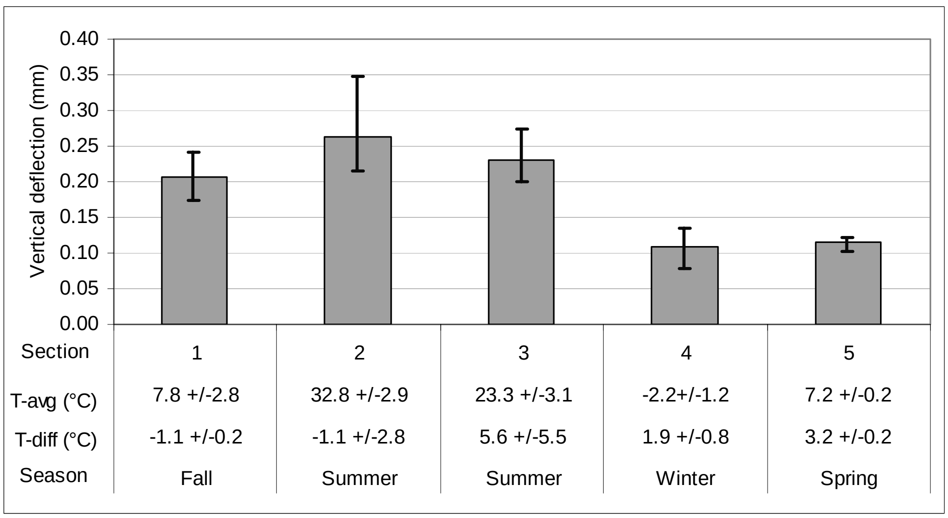

Figure 10. Rebound deflection at each section under 45kN

Sections 1, 2, and 3 consist of 254 mm thick slabs, and the deflections were approximately twice the deflections observed in the 356 mm thick slabs of sections 4 and 5. The additional reinforcement in section 3 (1.09 percent) with respect to sections 1 and 2 (0.55 and 0.80 percent respectively) did not significantly alter the elastic deflection measurements. At time of testing in section 2, the subgrade was saturated due to heavy rainfall, which could help to explain the higher deflections that this section experienced compared to sections 1 and 3. The 356 mm thick sections experienced similar deflections values to each other signifying the single versus double layer of steel arrangement did not affect the elastic responses.

Transverse cracks

All transverse cracks in the experimental sections developed naturally (as opposed to sections 6 to 10 where cracks were induced). The opening of the cracks was observed to vary with daily and seasonal temperature cycles, and through the thickness of the slab. More movement was measured near the surface than deeper in the slab. Changes in the average pavement temperature of the slab cause expansion and contraction of the concrete, while changes in the temperature difference produce rotation at the crack faces. Both linear and rotational movements affected the measured crack width. Daily changes in crack width of up to 0.09 mm were measured near the surface, while the movement close to the bottom of the slab was generally smaller than 0.03 mm.

Crack width was determined based on the closing movement of the upper half of the cracks under the action of the vertical load (Kohler and Roesler 2004b, 2005). Crack width cannot be compared from one section to another based only on the direct measurements because of the different temperature conditions in which each section was evaluated. Using calibrated formulas for each crack, the measured crack width was converted to a standard temperature of zero Celsius at the depth of the steel and zero temperature difference (Kohler 2005). The average crack width corrected for temperature and at the depth of the steel is shown in Table 2 along with information on the crack spacing of each section. Crack width in section 2 could not be obtained because the high temperatures of the summer kept the cracks fully closed. Crack widths on each section were smaller compared to values presented in the literature. The increased steel content from section 1 (0.55 percent) to section 3 (1.09 percent) effectively reduced the crack width. Section 4 was expected to have wider cracks than section 3 due to the lesser amount (0.78 percent) and deeper location of the reinforcement. However, crack widths were found to be smaller. Each section's average crack width comes from the measurement of four independent cracks, except for section 5 where there was only one crack to instrument.

Table 2. Average crack width and crack spacing

Section	Crack width (mm)	Crack spacing (m)				
	at depth of steel	Nr. of cracks	Average spacing	Min	Max	STDV
1	0.116	15	1.40	0.27	7.86	2.04
2	-	27	0.90	0.27	2.71	0.69
3	0.064	33	0.78	0.24	1.69	0.36
4	0.031	15	1.44	0.21	4.27	1.30
5	0.081 (1)	4	6.22	1.32	10.35	4.56

(1) depth corresponds to the average depth of the two layers of steel

The highest number of cracks occurred in section 3, which was in the middle of Lane 1 and had the largest steel content. The average crack spacing was 0.78 m. In section 2, the average crack spacing was 0.90 m, with the only difference in design between the two sections being the steel content. The additional steel in section 3 with respect to section 2 resulted in a reduction in the average crack spacing.

Section 1 had even less steel than section 2, and the average crack spacing increased to 1.40 m. Some movement likely occurred at the lug end of section 1, which had the effect of increasing the average spacing. It is not definitive whether the 1.40 m spacing corresponded to the true crack spacing of the section 1 due the unknown end effects. It is reasonable to expect that if section 1 had been at an interior location in Lane 1, the spacing would be between 0.90 and 1.40 m (greater than section 2 but smaller than observed). Crack spacing between 1.0 and 1.5 m are considered suitable for good performing CRCP, and therefore sections 1 to 3 can represent desirable field sections. Section 4 was 112 mm thicker and had approximately the same steel content as section 2, although the steel was placed deeper from the surface. Section 4 had half the number of cracks as section 2, and therefore it can be concluded that the two effects, thicker slab and greater steel depth, combined to generate a spacing of 1.44 m in section 4 that is considerably higher than the 0.90 m in section 2. Existing field data (Burke and Dhamrait 1968, Dhamrait et al. 1973) and models (Sato et al. 1989, Kim et al. 2001) show an increase in thickness and deeper reinforcement result in larger crack spacing. The cracking pattern in Section 5 was difficult to assess since only four cracks developed over the entire pavement length. The large crack spacing can be attributed to the lug movement at the end of Lane 1 and the effect of double layer steel placement. Crack spacing in all sections (except section 5) can be considered within a typical range of field CRCP.

Damaging loads and longitudinal cracking

Since the objective of the test was to understand the failure mechanism of CRCP, a large number of wheel passes were applied, some at very high load levels. This translated into longitudinal cracking in three of the five pavement sections. Section 4 did not develop longitudinal cracking even though the loading scheme was similar to sections 1, 2 and 3. Section 5 loading was completed to collect response data only, due to inability to fail section 4 which had the same thickness. Figure 11 presents the load history, total number of repetitions, estimated total ESALs applied and ESALs at time of the first failure. ESALs were calculated using load factor with a 4.3 exponential and an equivalent damage ratio of 20 to account for channelized trafficking of the ATLAS wheel at the pavement edge. The estimated ESALs at time of the first longitudinal crack was between 230 and 548 millions for the 254mm sections, and no damage occurred on section 4 (356mm) after 764 millions ESALs. The CRCP test sections performed much better than the predicted life based on the current AASHTO Design Guide (1993). For the 254mm and 356mm slab thicknesses, the expected CRC pavement life was predicted to be 6 and 50 million ESALs, respectively, using the AASHTO design procedure.

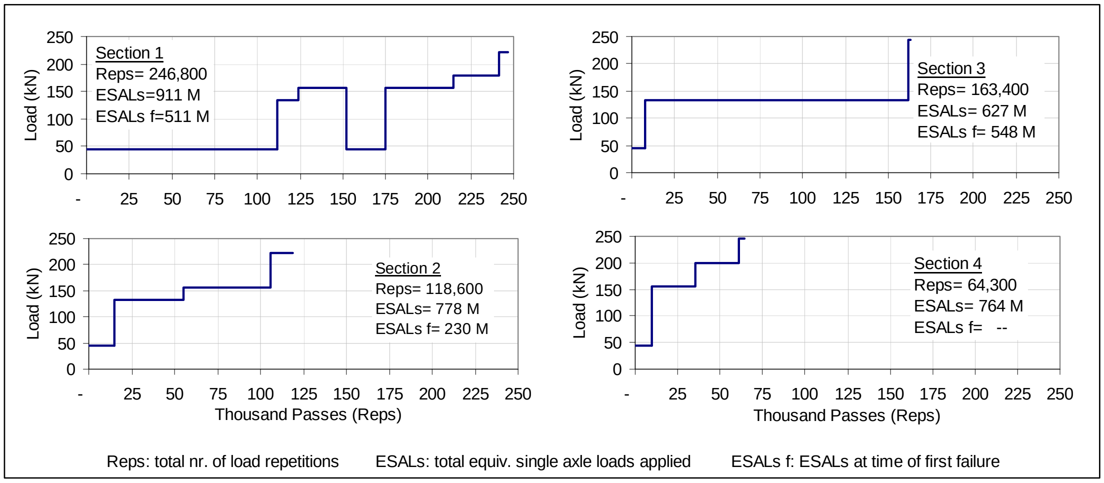

Figure 11. Load history, total ESALs, and ESALs at failure for each section

Longitudinal cracks initiated 1.2 to 1.5 meters from the loaded edge at transverse cracks and eventually propagated toward the pavement edge with the applications of more load repetitions. At the end of loading, they resembled half-moon cracks. The locations where the longitudinal crack extended to the edge in general coincided with longer panels. The presence of other closely spaced transverse cracks allowed the crack to continue propagating longitudinally through multiple transverse cracks. The half-moon cracks had the potential to develop faulting and the enclosed area was considered a punchout. A cascade effect created failures associated with the original punchouts, affecting a considerable length of the test section. The length of each punchout was between 3 and 14 m. Secondary longitudinal cracks formed closer to the edge in sections 1 and 2. Figure 12 presents the crack maps for all sections after the loading was finished.

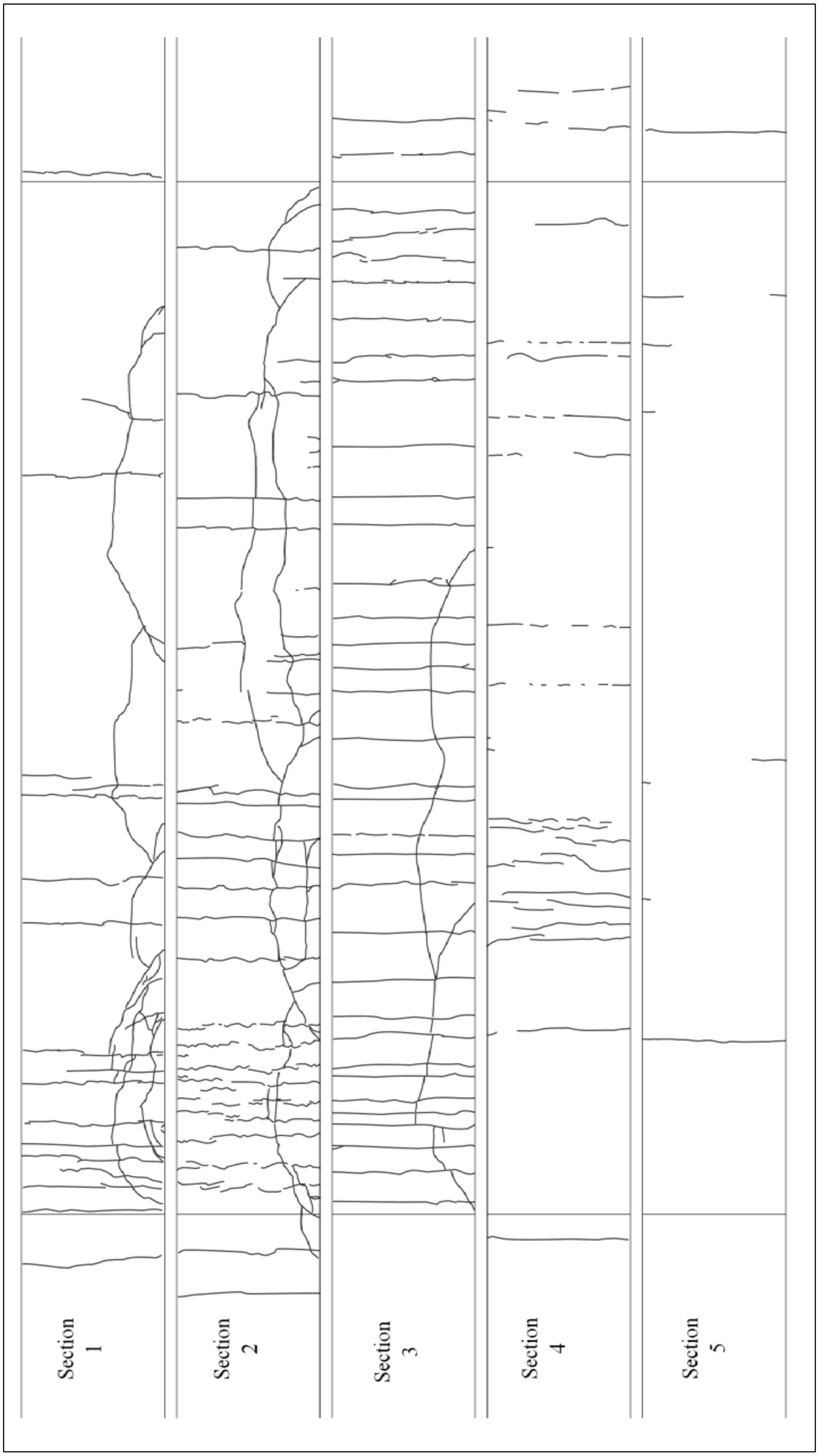

Figure 12. Crack maps at the end of loading.

The measurement of vertical deflection on both sides of each crack revealed that the load transfer across the cracks did not decrease as described in the traditional punchout failure mechanism for CRCP. Based on the observation of the vertical deflections, the longitudinal cracking was the result of permanent deformation under the slab, produced by the repetitive action of heavy wheel loads. The following analysis addresses the damage process in CRCP, neglecting temperature effects. The instrumentation setup allowed response measurements in the slab, while the exact deformations in the underlying layers can only be inferred from the collected data. The following three possible deformation scenarios represented in Figure 13 for CRCP are described below.

i) Elastic deformation in the slab and supporting layers: both maximum and unloaded vertical deflections remain the same after each wheel pass. Low load levels are being applied and no damage or permanent deformation is accumulating in the CRCP system.

ii) Elastic deformation in the slab and permanent deformation in the subbase: maximum deflections increase as more heavy-load repetitions are applied, but unloaded deflections remain unchanged because the slab returns to the original position after each load repetition. The increase in maximum deflection is related to the creation of permanent deformation or voids beneath the slab. The slab is progressively subjected to higher flexural stresses, and receives less support from the subbase to distribute the load.

iii) Permanent deformation in both slab and subbase: when the bending capacity of the slab is exceeded, the concrete fractures and seats in the subbase, with both the unloaded and loaded deflection increasing.

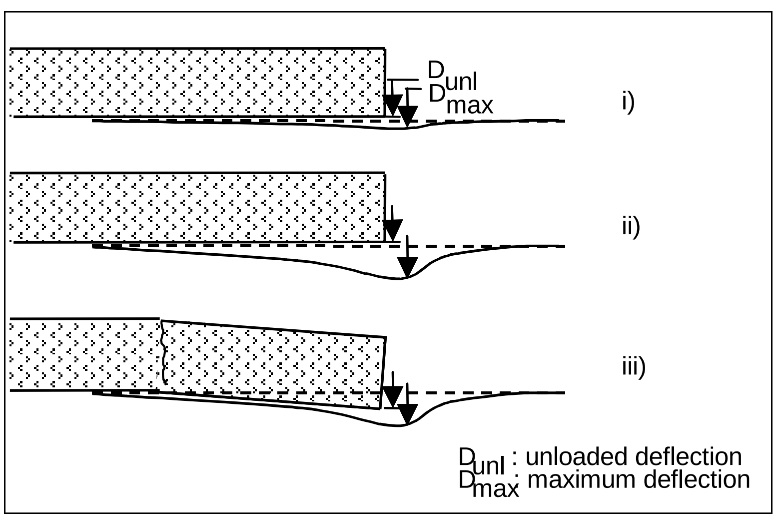

Figure 13. Vertical deformation at the edge of CRC pavement system

The longitudinal cracks started and developed with no decrease in load transfer efficiency across the transverse cracks. Traditionally, the loss of LTE is cited as the cause of the increased stresses that generate the longitudinal cracks. However, it was found that under small crack widths (see Table 2) the longitudinal cracks start and propagate without loss in transverse crack shear capacity (see Figure 14). The sequence of events that lead to faulted punchouts is described in Figure 15.

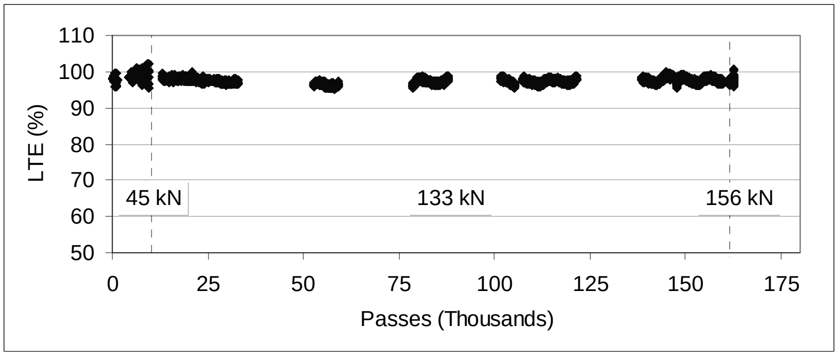

Figure 14. Load transfer efficiency throughout the testing at representative crack on section 2

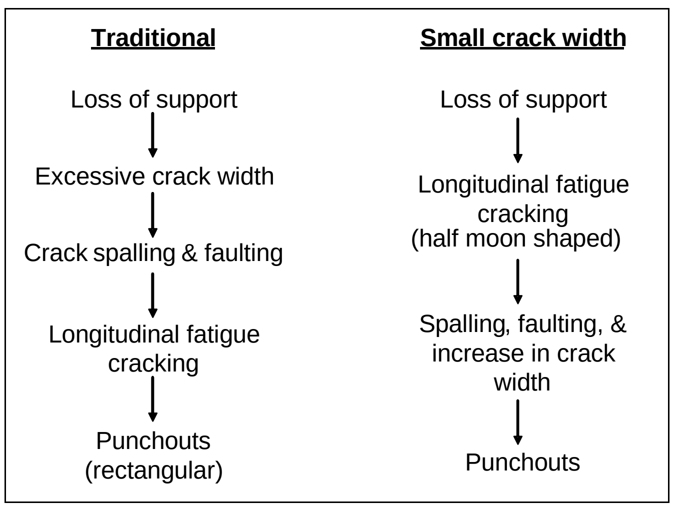

Figure 15. Traditional and small crack width sequence leading to faulted punchouts

The high elastic deformations experienced at the slab edge near transverse cracks caused permanent deformation of the supporting layers and a subsequent void beneath the slab, which eventually lead to the longitudinal cracking (punchout) failure. Permanent deformation was measured with a portable profilometer on section 1, as shown in Figure 16, and indicated that the slab ended up almost 20 mm below its initial position at the location of peak deformation. The rest of the test section also subsided under the repeated action of the wheel load. Figure 17 presents an estimation of the permanent deformation on section 2 based on unloaded deflection, and supports the finding from section 1.

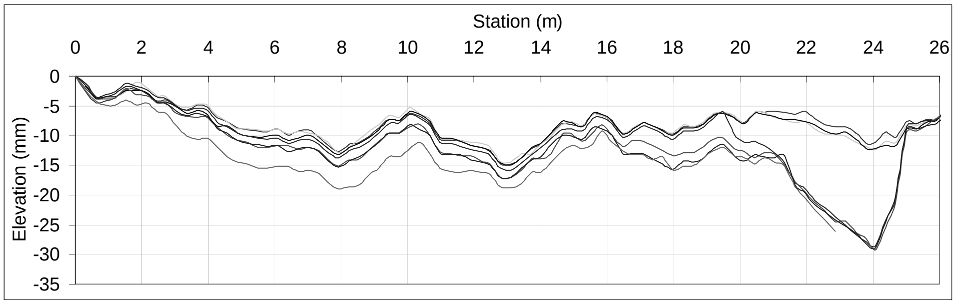

Figure 16. Longitudinal profile at the edge as loading progressed

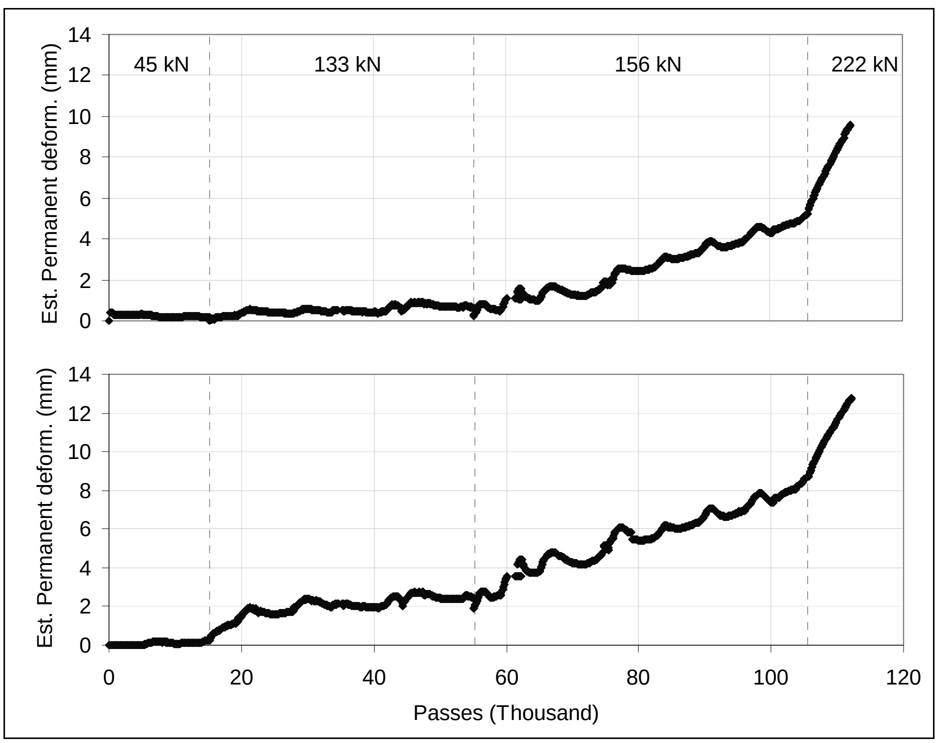

Figure 17. Estimated permanent deformation at two cracks in section 2

Conclusions

Five full-scale experimental sections of CRCP were instrumented and subjected to accelerated (heavy) traffic loading in order to measure pavement responses, compare different CRCP design features, and understand the failure mechanisms of CRCP. All measured responses (vertical deflections measured at the edge, the transverse strain obtained near the top of the slab, and the crack openings) were affected on a daily and seasonal basis by the thermal conditions of the slab, in particular by the difference in temperature through the concrete's thickness. The vertical deflection measured at the edge and transverse strains varied as much as 30 percent during a single day.

Crack width was measured at the edge of the slab based on the closing movement under increasing wheel loads. The average crack width was found to be in the range of 0.031 to 0.116 mm. Crack spacing ranged from 0.78 to more than 6.0 m. The crack width decreased with increasing steel content as observed from section 1 to section 3 (0.55% and 1.09% steel in 25 cm thick slabs) while section 4 unexpectedly had the smallest crack width even though it was a thicker slab with 0.8 percent steel content. The effect of steel content on crack spacing was difficult to assess because the lugs allowed some slab movement at the ends of Lane 1, decreasing the number of cracks on the sections located at both ends of the lane. Deflection measurements indicated, as expected, that the thicker sections experience less vertical deformation compared to the thin sections. It was not possible to identify significant differences in deflections between sections with different steel contents and the same thickness.

The performance of the CRCP sections under repeated loading revealed that under small crack widths (less than 0.15 mm), the shear load transfer capacities remained intact despite the heavy wheel loads. With small crack width, CRCP punchout failure (longitudinal cracking) was controlled by the permanent deformation in the supporting layers. The performance of the CRCP sections under accelerated loading exceeded by far the predicted life of the sections based on current CRCP design guides.

Acknowledgments

This material is based upon work supported by the Illinois Department of Transportation (IDOT) under the Illinois Cooperative Highway and Transportation Research Program No. IHR-R32. The financial assistance received from IDOT is greatly appreciated. Any opinions, findings, and conclusions or recommendations expressed in this publication are those of the authors and do not necessarily reflect the views of IDOT.

References

Burke, J.E., Dhamrait, J.S. (1968). *A Twenty-Year Report on the Illinois Continuously Reinforced Pavement*; Highway Research Record No. 239, Highway Research Board, pp197-211

Dhamrait, J.S., Jacobsen, F.K., and Schwartz, D.R. (1973). *Condition of Longitudinal Steel in Illinois Continuously Reinforced Concrete Pavements*, Physical Research Report No. 89 (IHR-36), Illinois DOT

Gharaibeh, N. G., Darter, M.I., Heckel, L.B. (1999). *Field Performance of Continuously Reinforced Concrete Pavement in Illinois*, Transportation Research Record - Journal of the Transportation Research Board 1684, pp 44-50.

Kim, S-M., Won, M.C., McCullough, B.F. (2001). *CRCP-9: Improved Computer Program For Mechanistic Analysis of Continuously Reinforced Concrete Pavements*. Research Report FHWA/TX 0-1831-2, 116p

Kohler, E.R. (2005). *Experimental Mechanics of Crack Width in Full-Scale Sections of Continuously Reinforced Concrete Pavements*. PhD Dissertation, University of Illinois at Urbana-Champaign.

Kohler, E.R. and Roesler, J.R (2004a). *Active Crack Control for Continuously Reinforced Concrete Pavements*, Transportation Research Record 1900, Journal of the Transportation Research Board, Washington, D.C., pp. 19-29.

Kohler, E.R. and Roesler, J.R (2004b). *Crack Width Determination in Continuously Reinforced Concrete Pavements*, Proceedings of the Second International Conference on Accelerated Pavement Testing (CD-ROM), Minnesota, September 2004.

Kohler, E.R. and Roesler, J.R. (2005). *Crack Width Measurements in Continuously Reinforced Concrete Pavements*, in press, September, ASCE Journal of Transportation Engineering.

Poblete, M., Salsilli, R., Valenzuela, R., Bull, A., and Spratz, P. (1988). *Field Evaluation of Thermal Deformations In Undoweled PCC Pavement Slabs*. Transportation Research Record - Journal of the Transportation Research Board 1207, pp 217-228

Sato, R., Hachiya, Y., Kawakami, A. (1989). *Development of New Design Method for Control of Cracking in Continuously Reinforced Concrete Pavement*. Proceedings, 4th International Conference on Concrete Pavement Design and Rehabilitation, Purdue University, April 18-20. Report FHWA-RD-89-208 pp 431-443

Smith, K. D., Wade M. J., Peshkin D. G., Khazanovich L., Yu H. T., Darter M. I., (1998). *Performance of Concrete Pavements, Vol. II: Evaluation of in-service Concrete Pavements*. FHWA-RD-95-110

Won, M. (2005). *Improvements of Testing Procedures for Concrete Coefficient of Thermal Expansion.* Proceedings Transportation Research Board 84th meeting (CD-ROM), Washinton D.C. paper nr. 05-2521